Nonlinear analyses of steel beams and arches using virtual unit moments and effective rigidity

Lenka Koubova*[1], Petr Janas [1a], Alexandros Markopoulos [2b] and Martin Krejsa [1c]

[1] *Department of Structural Mechanics, Faculty of Civil Engineering, VSB - Technical University of Ostrava,
Ludvika Podeste 1875/17, 708 33 Ostrava-Poruba, Czech Republic*
[2] *Department of Applied Mathematics, IT4Innovations, VSB - Technical University of Ostrava,
Studentska 1, 708 33 Ostrava-Poruba, Czech Republic*

Abstract. This study examined geometric and physical nonlinear analyses of beams and arches specifically from rolled profiles used in mining and underground constructions. These profiles possess the ability to create plastic hinges owing to their robustness. It was assumed that displacements in beams and arches fabricated from these profiles were comparable with the size of the structure. It also considered changes in the shape of a rod cross-section and the nonlinearities of the structure. The analyses were based on virtual unit moments, effective flexural rigidity of used open sections, and a secant method. The use of the approach led to a solution for the "after-critical" condition in which deformation increased with decreases in loads. The solution was derived for static determinate beams and static indeterminate arches. The results were compared with results obtained in other experimental tests and methods.

Keywords: steel structure; arch; beam; large displacement; geometrical nonlinearity; physical nonlinearity; virtual unit moments; effective flexural rigidity; open section; secant method

1. Introduction

Several previous studies (Kala *et al.* 2015, Janas *et al.* 2014, Kralik 2014, Janas *et al.* 2017, Randyskova and Janas 2011) focus on nonlinear solutions of structures. It is necessary for each structure to fulfill certain functions and to be specific and unique. Geometric nonlinear tasks are typically used for relatively small deformations (that is, for second-order tasks). A few studies have considered physical nonlinear tasks or geometric nonlinear tasks with deformations, which are significant with respect to the structure size. Other studies describe tasks with large deformations where changes in the profile shape of a structure and shape of a cross-section account for physical nonlinearities. Such types of structures are typically unacceptable and undesirable because the structure cannot be used. Fig. 1 shows an example of the deformation of a mining steel arch support from special profiles with abilities to create plastic hinges with changes in the shape of the cross-section.

Several extant studies focus on nonlinear analyses of arches. Pi *et al.* (2002) focused on the in-plane stability of arches. A study presented by Pi and Trahair (2000) investigated inelastic lateral buckling strength and design of steel arches under general loading using an advanced nonlinear inelastic finite element analysis method. Another study presented by Bradford (2006) considered nonlinear in-plane behavior of a circular arch subjected only to thermal loading. A nonlinear formulation of the strain-displacement relationship was used to apply the principle of virtual work to produce differential equations of in-plane equilibrium as well as static boundary conditions that govern structural behavior under thermal loading. An extant study presented by Pi and Bradford (2010) examined the effects of prebuckling response on buckling load determination of pin-ended elastic circular arches that were subjected to a uniform radial load. A generic non-linear inelastic mechanical-based formulation for a steel arch subjected to uniformly distributed loads at elevated temperatures was developed by Heidapour *et al.* (2010). Additionally, a study presented by Pi and Bradford (2013) discussed nonlinear elastic in-plane analysis and buckling of pin-ended arches with elastic rotational end restraints of unequal stiffness under a uniform radial load.

---

*Corresponding author, Ph.D.,
E-mail: lenka.koubova@vsb.cz
[a] Doc., E-mail: 1.petr.janas@seznam.cz
[b] Ph.D., E-mail: alexandros.markopoulos@vsb.cz
[c] Professor, E-mail: martin.krejsa@vsb.cz

Fig. 1 Deformed mining support (Janas 2008)

Several studies conducted nonlinear analyses of concrete filled steel tube (CFT) structures. The mechanical behaviors of CFT structures were investigated by nonlinear FEM analysis in a study presented by Xu *et al.* (2010). Furthermore, two and three-dimensional nonlinear finite element models were developed to study force transfer between a steel tube and a concrete core in a previous study presented by Starossek *et al.* (2010), and a nonlinear finite element program (ABAQUS) was used. Material and geometric nonlinearities of concrete and steel were considered in this analysis. The CFT components were widely used as the arch ribs of the long span arch bridges. With respect to nonlinear finite element model analysis, hysteretic behaviors of CFT arch ribs under the action of reduplicative load were investigated by extant research (Ma *et al.* 2015).

The present study considered geometric and physical nonlinear models and also described the use of virtual unit moments for tasks in which displacement was negligible with respect to dimensions of the structure. With respect to these tasks, the cross-section of the profile also changed its shape. The model was based on derived curves of effective flexural rigidity for a used open steel profile (Markopoulos *et al.* 2010).

The open rolled profiles were mainly used for arch supports, which are widely used in long workings in coal and ore mines (Krejsa *et al.* 2013) and in driven tunnels and galleries. They are designed to possess a sufficient plastic reserve and withstand large displacements. These profiles are significantly more complex from a geometric viewpoint when compared with profiles applied in steel constructions of buildings and civil engineering structures. The yield point of a material often exceeds when mining reinforcements are used. Hence, with respect to these cases, it is necessary to consider physical nonlinearity and the change of the shape of the profile, which occurs due to the action of bending moments and axial forces (eventually due to the torsion moments). Finite element method can be used to solve for entire sets of the mining arch (including geometric and physical nonlinearities as well as changes in the shape of the applied rolled profile). However, this task is relatively large for modeling a series of possible status that may occur in conditions in situ. Therefore, the modeling was explored on two levels. The values of effective flexural rigidity were obtained by FEM modeling in the first level. In the second level, beams and arch supports were
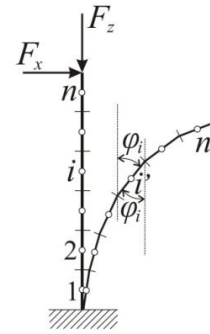
Fig. 3 The original rod and deformed rod, approximation of the rod by line segments

solved using effective flexural rigidity and the procedure described in the present study.

Supports of those and similar open profiles with different weights per meter were supplied in shapes required by customers such as ArcelorMittal Ostrava a.s. or by other manufacturers (Fig. 2). Complete sets of mine supports from open profiles were tested in special test facilities. Results of theoretical analyses presented in the study could replace these tests to a considerable extent.

2. Application of the virtual unit moments

For purposes of simplification, it was assumed that rods were fabricated from a linearly elastic material. In this case, the modeling involved a physically linear and statically determinate task. The steps were described with respect to a simple fixed rod (Fig. 3).

Based on finite deformation theory, equilibrium conditions were specified for a deformed structure. The model accounted for the influence of displacement and angular rotation on the magnitude of the force variable. In terms of the order of magnitude, the deformation was comparable with the rod lengths. The calculation was based on virtual unit moments and iteration.

The length of a rod was divided into n identical line segments. If the angular shift of the centre of each segment was known, then the gradual displacement of each point in the segment (including the end point of the segment) could be calculated, and in turn, the strain in the entire rod could be calculated. In order to calculate the angular rotation of the centre of each ith segment ($i = 1, …, n$), it was necessary to define the moment and normal force caused by the specified load: $M_{0,i}$, $N_{0,i}$. Next, a unit virtual moment was placed in the centre of each segment. The unit moment $M_{1,j} = 1$ loaded the centre of the jth segment, and indicated the moment $M_{1,i,j}$ and normal force $N_{1,i,j}$ in each ith segment. The moments and normal forces were counted for the deformed rod. The angular rotation for the centre of the jth segment is given by numerical integration as follows

$$\varphi_j = \int_0^l \frac{N_{1,j} N_0}{EA} ds + \int_0^l \frac{M_{1,j} M_0}{EI} ds$$
$$= \sum_{i=1}^n \frac{N_{1,i,j} N_{0,i}}{(EA)_i} ds_i + \sum_{i=1}^n \frac{M_{1,i,j} M_{0,i}}{(EI)_i} ds_i,$$
(1)

Fig. 2 Profile P-28 supplied by ArcelorMittal Ostrava a.s., Czech Republic

where *EI* denotes flexural rigidity of the rod and *A* denotes cross-section area of the rod. The influence of shearing forces on the deformation of the rod was ignored. Additionally, it was assumed that torsion moments did not exist. Eq. (1) can be modified for the unchanging cross-section as follows

$$\varphi_j = \sum_{i=1}^{n} \frac{N_{1,i,j} N_{0,i}}{EA} ds_i + \sum_{i=1}^{n} \frac{M_{1,i,j} M_{0,i}}{EI} ds_i \qquad (2)$$

When the angular rotation of each segment was derived, it was possible to calculate the normal force N_i and use Hooke's law to calculate the new length of each segment ds_i. Following the 1st iteration, the angular rotation and length were derived for each ith segment. Thus, the new coordinates could be specified.

The starting point corresponded to the point where the rod was fixed (that is, where the angular displacement corresponded to zero), and the final point corresponded to the free end. Using goniometric functions, it was possible to specify the coordinates of the centre of each ith segment x_i and z_i as well as the coordinates for its ends, that is, $x_{e,i}$ and $z_{e,i}$, as follows

$$x_i = x_{e,i-1} + \frac{ds_i}{2} \cdot sin\,\varphi_i,$$
$$x_{e,i} = x_{e,i-1} + ds_i \cdot sin\,\varphi, \qquad (3a)$$

$$z_i = z_{e,i-1} + \frac{ds_i}{2} \cdot cos\,\varphi_i,$$
$$z_{e,i} = z_{e,i-1} + ds_i \cdot cos\,\varphi, \qquad (3b)$$

The difference between the new coordinates, namely x_i and z_i, and the original coordinates, namely $x_{0,i}$ and $z_{0,i}$, could be used to derive horizontal and vertical displacements of centers of the ith segments u_i and w_i, respectively, and their corresponding end points, $u_{e,i}$ and $w_{e,i}$, as follows

$$u_i = x_i - x_{0,i}, \qquad w_i = z_i - z_{0,i}, \qquad (4a)$$

$$u_{e,i} = x_{e,i} - x_{0,e,i}, \qquad w_{e,i} = z_{e,i} - z_{0,e,i}, \qquad (4b)$$

Following the first calculation, new coordinates, namely x_i and z_i, represented the first approximation of the correct values corresponding to the load. It was necessary to perform the calculation several times for the deformed structure until the geometry of the loaded rod became stable. The measure of correctness for the calculation corresponded to the specified accuracy ε, which was based on the relative change of deformation parameters, namely $u_{i,k}$ and $w_{i,k}$, in the kth iteration and in the previous $(k-1)^{th}$ iteration as follows

$$\varepsilon = \frac{u_{i,k} - u_{i,k-1}}{u_{i,k}}, \qquad resp. \qquad \varepsilon = \frac{w_{i,k} - w_{i,k-1}}{w_{i,k}}. \qquad (5)$$

In this case, it was recommended that the changes at the point where the effect of the forces was maximized should be monitored. The progress of the iteration is shown in Fig. 4.

In the angular rotation calculation $\varphi_{i,k}$, the calculation could be accelerated (i.e. the number of iterations could be reduced) by means of a relaxation coefficient η. Thus, the modified angular rotation of the ith segment in the kth iteration $\varphi_{mod,i,k}$ is obtained as follows

$$\varphi_{mod,i,k} = \eta \cdot \varphi_{mod,i,k-1} + (1 - \eta) \cdot \varphi_{i,k} \qquad (6)$$

As shown in Fig. 4, the number of iterations reduces considerably if the relaxation coefficient η is not zero. If $\eta = 0$, then the full value of deformation is calculated in the kth iteration, and u & w approach a certain value. However, the convergence is very slow. For $\eta = 0.5$, the values of u and w stabilized rapidly at the final value.

The optimum value of the relaxation coefficient η was different in each case. The coefficient η ranged between 0 and 1. The value of the relaxation coefficient was optimized using software for more complex tasks.

The application of virtual unit moments was used in several cases as described in book presented by Kolar (1985) (NODEF2 method based on FEM). An accurate

Table 1 Results

	u [m]	w [m]	φ [rad]
Accurate value	0.90516	0.16929	0.46135
NODEF2, $k = 2$	0.90300	0.17100	0.46600
VUM, $k = 7$	0.90346	0.16833	0.45936
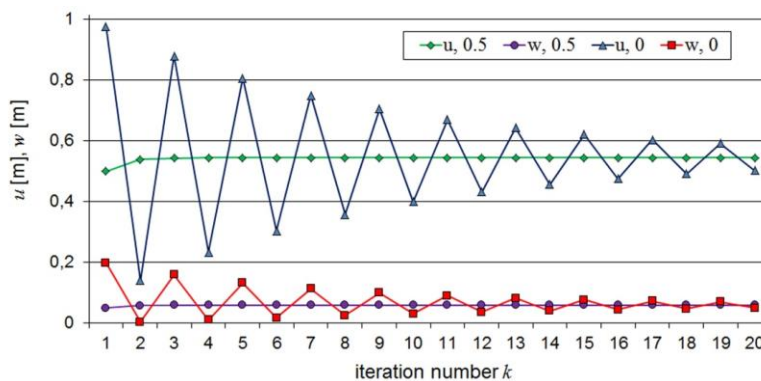
Fig. 4 Number of iterations versus the coefficient η ($\eta_1 = 0.5$, $\eta_2 = 0$)

solution was obtained by K. Mattiasson by using the elliptic integral. The same solution was also explored by Mattiasson (1981), where the fixed rod was loaded with only a single horizontal force F_x with the same direction at the free end (Fig. 3). Table 1 shows the deformation at the free end of the rod for a rod length of $l = 3$ m, flexural rigidity of $EI = 1749.93$ kNm^2, and horizontal force of $F_x = 194.436$ kN. The deformation calculated for the free end of the bracket as shown in Table 1 proved that modeling with virtual unit moments ("VUM" - as also shown in Table 1) could be considered accurate. The rod was divided into 10 segments. The minimum required accuracy corresponded to $\varepsilon = 10^{-5}$. In Table 1, k denotes the number of iterations.

3. Effective flexural rigidity

In the following chapters, it was not assumed that the rods were made from a linearly elastic material. Thus, modeling was physically nonlinear in these cases. The changes in the shape of a rod cross-section accounted for the physical nonlinear solution. These changes occurred due to the action of bending moments and normal forces and potentially even due to the torsion moments.

The values of the effective flexural rigidity were obtained by using the finite element method (FEM). The values of the effective flexural rigidity were a function of internal forces. These values were used in the solution of beams and potentially even in the solution of mining steel arch supports in the following chapters.

The FEM modeling of the P-28 and TH-29 profiles was based on the dimensions of these profiles that were commonly available in prospectuses provided by the manufacturers of mining reinforcement. A three-dimensional model was created using ANSYS software (see in Fig. 5(a)). A standard 3D brick element with eight nodes was used (see in Fig. 5(b)). The computer modeling allowed the inclusion of material non-linearity and the changes in the shape of the profile in the calculation.

The simple tri-linear kinematic hardening model was used for the calculation. The deformation characteristic was replaced by the polyline as shown in Fig. 6. The parameters of the tri-linear model of plasticity were derived from the results of the tensile test of the applied steel.

A unilaterally fixed beam was chosen for the analysis of the flexural rigidity. This fixed beam was loaded by a pair of forces on the free end. Additionally, the beam could also be loaded by a normal force and eventually by the torsion moment (as shown in Fig. 7).

The rotation angle of the free end Φ is given by the following equation

$$\Phi = \frac{M \cdot l}{EI} \qquad (7)$$

where M denotes the bending moment, l denotes the length of the beam, E denotes the modulus of elasticity in tension,
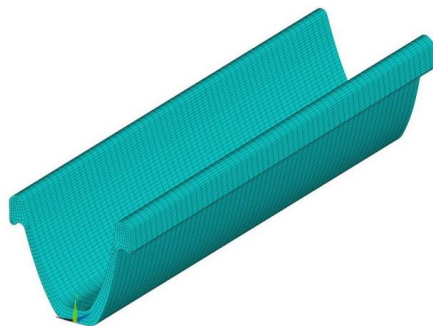
(a) The model of the profile
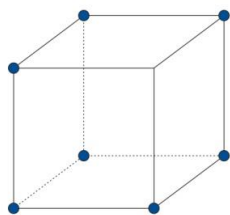
(b) The standard 3D brick element (8 nodes)

Fig. 5 The model of the profile and the standard 3D brick element (8 nodes)
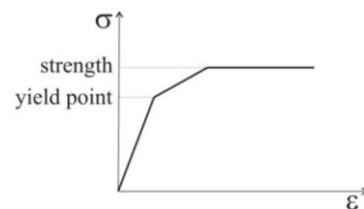
Fig. 6 The tri-linear model of plasticity
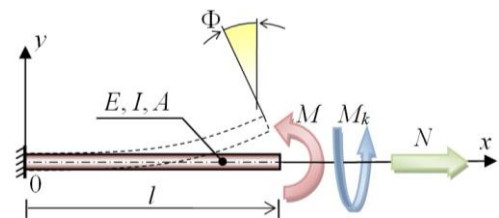
Fig. 7 The bending of a perfectly fixed beam
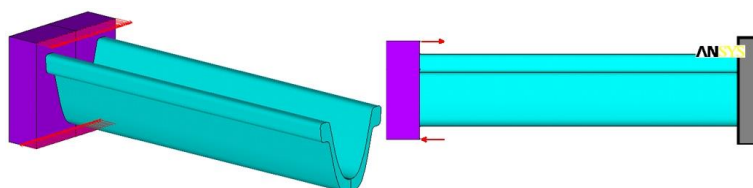
Fig. 8 Loading of the beam with a pair of forces

and I denotes the moment of inertia.

The bending moment M could not be directly introduced in the "finally-elementary" model. Therefore, a cube with high rigidity was added to the free end of the profile model. A pair of forces acted at the edges of the cube. This pair of forces in an arm produced the bending moment (as shown in Fig. 8).

The forces on the upper and lower edges of the cube did not directly enter the calculation, but their displacements were part of the calculation. The forces were subsequently detected as a response. This was due to the convergence of the solution despite overcoming the top characteristics when the "softening" occurred (see in Fig. 9(a)). The output of the calculation corresponded to the gradually increasing rotation angle Φ and the corresponding bending moment M.

The dependence of bending moment M on the rotation angle Φ represents the bending characteristics. An initial linear section could be observed (this corresponded to the linear theory of beams). A slow increase in the bending moment was then observed (as a result of plastication and later as a result of changes in the profile). A significant opening of the profile was observed at the rotation angle approximately at $\Phi = 17$ degrees, and it thereby reduced the stiffness. Less bending moment is then required to further the bending of the profile. This point represented the loss of stability of the profile shape. The next bending-rotation was possible only at lower loads. The same loading could result in the collapse of the construction.

This phenomenon was associated with the change (reduction) of the flexural rigidity. The effective flexural rigidity of the cross section could be determined from Eq. (7). The effective flexural rigidity EI was a function of the bending moment and is given as follows

$$EI_{(M)} = \frac{M \cdot l}{\Phi} \qquad (8)$$

The effective flexural rigidity was constant when the loading corresponded to a certain value (see in Fig. 9(b)), and it corresponded to the product of the modulus of elasticity (denoted as E) and the moment of inertia (denoted as I). The effective flexural rigidity decreased as a result of the plastication, and later as a result of reductions in the moment of inertia of the profile. The transition point represented the loss of stability of the profile shape. It was also clear from Fig. 9(b) that two values of the effective flexural rigidity corresponded to a value of the bending moment (even though the normal force corresponded to zero).

The introduced calculation referred to the beam stressed with only the bending moment. If the normal force also acted on the beam, then the bending moment was not generally linear along the beam. In this case, it was advantageous and practically necessary to divide the analyzed beam along the cuts with an equidistant step.

Thus, the change in the rotation of the cut i is given as follows

$$\Delta\varphi_i = \frac{M_i \Delta L_i}{(EI)_i} \qquad (9)$$
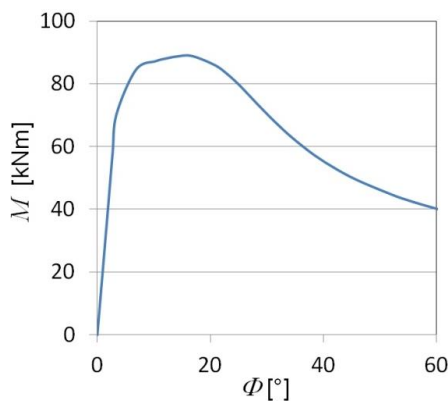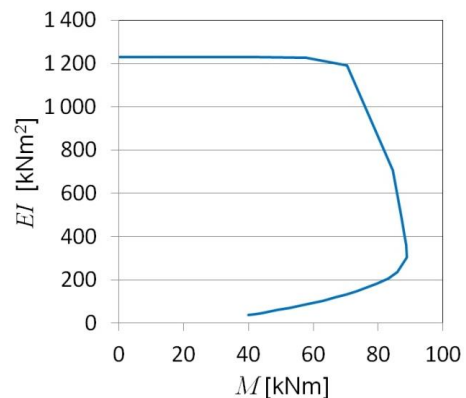
(a) The bending characteristics (TH-29)   (b) Effective flexural rigidity as a function of M

Fig. 9 The bending characteristics (TH-29) and effective flexural rigidity as a function of M
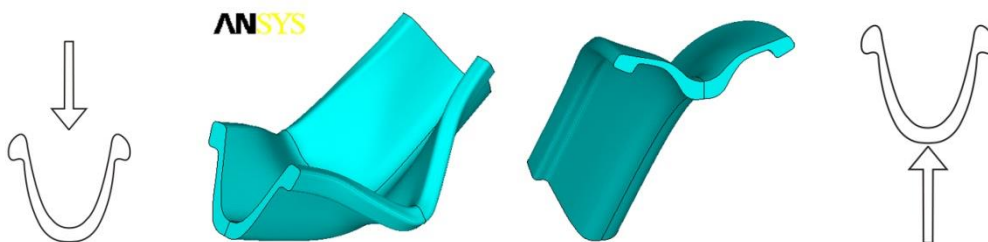
Fig. 10 The deformation of the bending profile, the load is applied to the profile as shown on the left and the root profile as shown on the right

The equivalent flexural rigidity $(EI)_i$ of the cut i corresponded to the length of the cut of the beam ΔL_i and the change in the rotation $\Delta \varphi_i$ when a known bending moment M_i is as follows

$$(EI)_i = \frac{M_i \Delta L_i}{\Delta \varphi_i} \qquad (10)$$

If this ratio is marked, then it results in the following equation

$$d\varphi_i = \frac{\Delta \varphi_i}{\Delta L_i} \qquad (11)$$

The effective flexural rigidity of the beam in the cut i is given as follows

$$(EI)_i = \frac{M_i}{d\varphi_i} \qquad (12)$$

The solved profiles were symmetrical, but they were also open. As a result, they transmitted different bending characteristics when the loading with the bending moment corresponded to "to the profile" or "on the root of the profile" (as shown in Fig. 10). The solved TH-29 profile was more stable and could carry a greater bending moment when the loading corresponded to "on the root of the profile". The character of deformation of the TH-29 profile was evident from Fig. 10 when the loading corresponded to "to the profile" (left) and "on the root of the profile" (right).

The values of effective flexural rigidity could be expressed graphically as functions of the bending moment for a variety of normal forces (as shown in Fig. 11) or in the form of a data file. The effective flexural rigidity EI is on the vertical axis and the bending moment M is on the horizontal axis as shown in Fig. 11. The values of the bending moment were positive for the load acting on the profile and negative for the load acting on the root of the profile. As clearly shown in Fig. 11, the tensile normal forces stabilized the profile. The pressure (negative) normal forces reduced the stability of the profile and its effective flexural rigidity contrary to expectations.

The disadvantage of a data file corresponding to the Fig. 11 was that two values of effective flexural rigidity of the profile corresponded to a value of the bending moment for a given value of normal force. This fact complicated the calculation in the algorithm by using the introduced data. Hence, the data files were processed such that the effective flexural rigidity was expressed as a function of the relative rotation (curvature) of the profile (as shown in Fig. 12). Only one value of effective flexural rigidity corresponded to a value of relative rotation for a given normal force. Hence, using effective flexural rigidity was advantageous for the nonlinear solution.

The profile of mining reinforcement could also be loaded by torsion moments. The course of a curve of the effective flexural rigidity was practically the same in the flexible area and in the partial plastication of the profile when the load was applied to the profile despite the existence of the torsion moments (as shown in Fig. 13). However, the value of the maximum bending moment that the profiles can transfer while the load torsion moments, decreases. The effective flexural rigidity practically did not change with the existence of the torsion moments when the load was applied on the root of the profile. The value of the effective flexural rigidity for a given value of relative rotation $d\varphi$ was lower when a mixed loading with bending and torsion moments was applied as shown in Fig. 13 (the
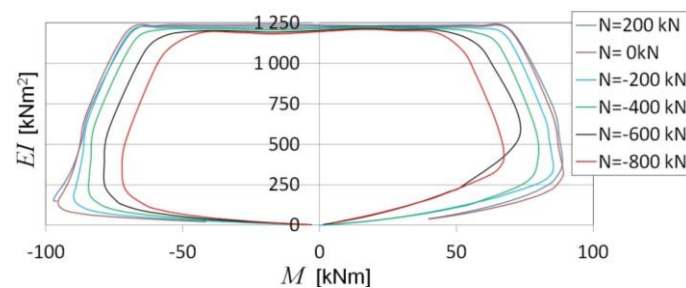
Fig. 11 The effective flexural rigidity of TH-29 profile manufactured from H500M steel as a function of the bending moment for a variety of normal forces
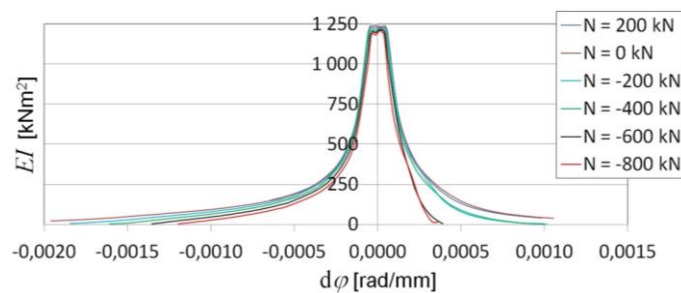
Fig. 12 The effective flexural rigidity of TH-29 profile manufactured from H500M steel as a function of relative rotation for a variety of normal forces
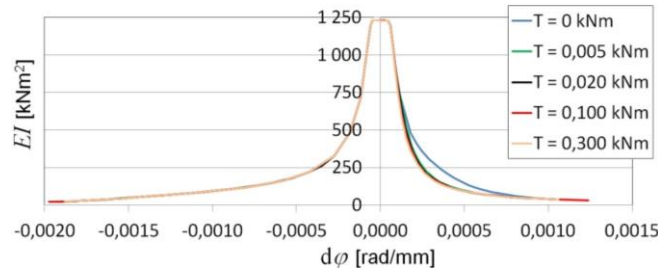
Fig. 13 The effective flexural rigidity of TH-29 profile manufactured from H500M steel as a function of relative rotation (curvature) for a variety of torsion moments
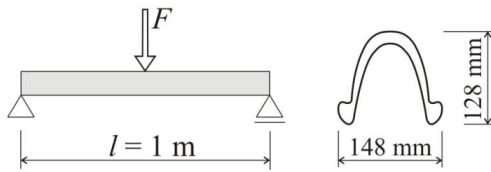
Fig. 14 The beam and profile P-28

load was applied to the profile). From this standpoint, it was advisable to design the steel arch support such that the possibility of the origin of torsion moments was minimized.

4. Application of virtual unit moments for the validation of flexural test results

Virtual unit moments could be used after a bending test of a beam to model physical nonlinear tasks with changes in the shape and thereby to model the rigidity of the profile.

The beam had a length of 1 m and had a P-28 profile (as shown in Fig. 14). The beam was divided along its length into n segments. The beam was loaded and deformed. In the middle of the beam, the specified vertical displacement corresponded to w_s, and it was necessary to find the

corresponding loading force, namely F. Until the maximum force F_{max} was reached, the loading force increased with increases in the displacement w_s. Subsequently, the loading force decreased with increases in the displacement w_s due to the physical nonlinear behavior of the material and the changes in the profile shape. The deformation load was selected such that the force F could be derived even after F_{max} was reached.

The displacement was calculated iteratively. The initial values for the vertical force F_k were selected for $k = 0$ and $k = 1$ for each specified displacement w_s. In the case of the iterations that corresponded to the zeroth and first iterations, the calculation described in the above chapter was used for the angular displacement and thereby for the coordinates of each segment. The secant method was applied for the calculation of the next vertical force, i.e. beginning with $k = 2$ (generally, after the kth iteration, the force corresponded to F_{k+1}). The vertical force was a function of the vertical displacement of the beam centre in the kth iteration $w_{s,k}$ and in the $(k-1)^{th}$ iteration $w_{s,k-1}$ as follows

$$F_{k+1} = F_k - \left(w_{s,k} - w_s\right) \cdot \frac{F_k - F_{k-1}}{w_{s,k} - w_{s,k-1}}. \qquad (13)$$

The steps were repeated until the relative change in F_{k+1}
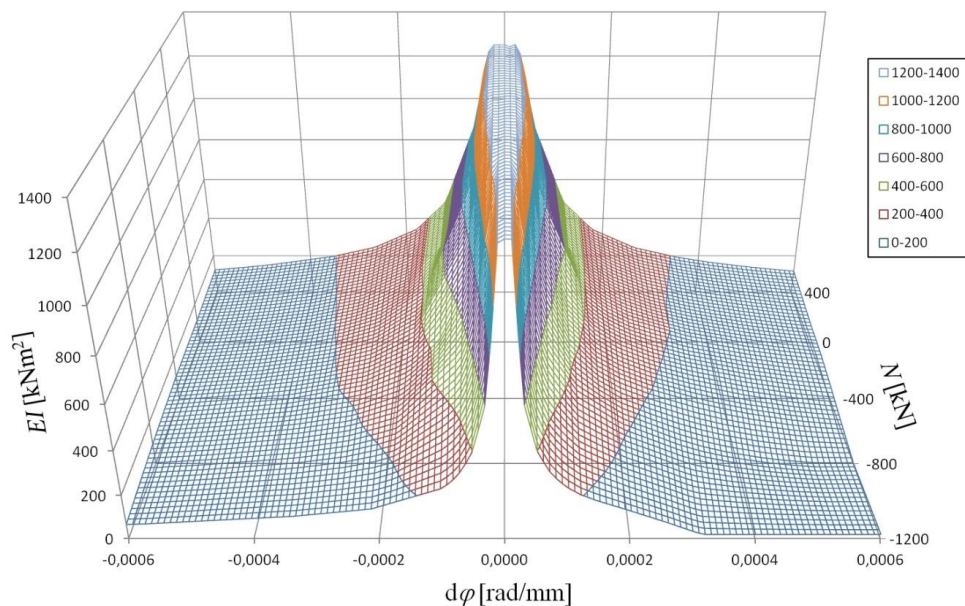
Fig. 15 A 3D graph of effective flexural rigidity in the P-28 profile

reached the specified accuracy as denoted by ε_1. Simultaneously, the specified displacement (denoted as w_s) was compared with the calculated vertical displacement (denoted as $w_{s,k+1}$) in the middle of the beam as follows

$$\left|\frac{F_{k+1} - F_k}{F_{k+1}}\right| \leq \varepsilon_1, \quad \text{resp.} \quad \left|\frac{w_{s,k+1} - w_s}{w_s}\right| \leq \varepsilon_1. \quad (14)$$

The modeling was both geometrically nonlinear and physically nonlinear, and thus, the calculated force F_{k+1} did not correspond to the final result for the specified deformation w_s even after ε_1 was reached. Once F reached the specified accuracy, it was important to check and modify the flexural rigidity of the segments $(EI)_i$.

Fig. 15 shows a 3D graph of the effective flexural rigidity EI of the profile P-28. The curves denote a function of the relative angular displacement $d\varphi$ and depended on the normal force N. As previously mentioned, FEM was used (Markopoulos *et al.* (2010)). Similar curves were obtained from experimental flexural tests for the zero normal force (Randyskova and Janas 2010).

The relative angular displacement $d\varphi_i$ of the centre of each segment (denoted as i) was determined to deduce the flexural rigidity of each segment.

$$d\varphi_i = \frac{\varphi_{i+1} - \varphi_{i-1}}{2 \cdot ds_i} \quad (15)$$

If the normal force corresponded to zero, then this value corresponded to the effective flexural rigidity of each segment $(EI)_i$. The values of the effective flexural rigidity

were processed in a table where they were deducted directly or they were obtained through interpolation. A shift of centre of the beam w_s altered the effective rigidity of the segment and thereby altered the loading force F. The exact value was again obtained by iterations for the specific effective flexural rigidity. If Eq. (14) was satisfied following the change in the flexural rigidity, then the calculation was completed for the specified w_s. Otherwise, the steps were repeated to improve the accuracy of the force F and thereby improve the flexural rigidity. When the specified accuracy ε_1 was reached and the flexural rigidity was altered for the segments for w_s, the calculation continued with the increased value of w_s.

Fig. 16 shows the loading results from the internal and external sides of the profile and compares the same with the data obtained from the flexural test of the P-28 profile (Grochol 1996). The charts indicated good correlation between the flexural tests and calculations as based on the virtual unit moments and effective flexural rigidity. The calculations were performed with the specified accuracy corresponding to $\varepsilon_1 = 10^{-5}$.

5. Application of the virtual unit moments that load the arch support with a vertical force

The solved two-joint circular arch corresponded to a once statically indeterminate structure. The system of coordinates was chosen pursuant to Fig. 17 in which the origin corresponded to the top of the unloaded arch. The arch was divided along its length into n line segments. Each
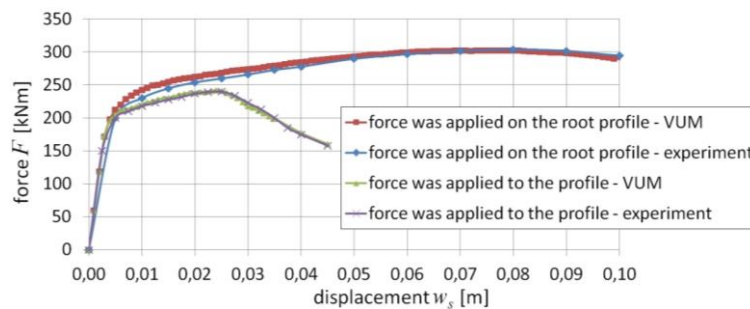
Fig. 16 The situation after the deformation is applied on the internal and external sides of the profile
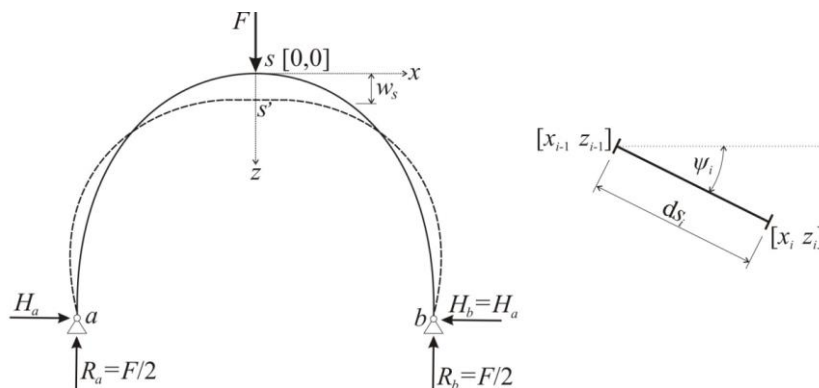
Fig. 17 The arch and the segment i

segment was defined by its length ds_i, slope ψ_i, and coordinates of nodal points, that is, the end points of each segment.

The arch was loaded and deformed. If the specified vertical displacement at the arch top corresponded to w_s, then it was necessary to find F and the responses R_a, R_b, H_a, and H_b, as shown in Fig. 17.

The horizontal response $H_a = H_b$ was a function of the displacement u_b in the right support, which corresponded to zero if the joint support b did not shift (the displacement corresponded to zero) as follows

$$H_{a,k+1} = H_{a,k} - (u_{b,k} - u_b) \cdot \frac{H_{a,k} - H_{a,k-1}}{u_{b,k} - u_{b,k-1}}$$
$$= H_{a,k} - u_{b,k} \cdot \frac{H_{a,k} - H_{a,k-1}}{u_{b,k} - u_{b,k-1}}. \tag{16}$$

The vertical force F was calculated in a manner similar to that in the previous section pursuant to Eq. (13).

The iteration was repeated until H_a and F reached the specified accuracy ε_1 as follows

$$\left| \frac{H_{a,k+1} - H_{a,k}}{H_{a,k+1}} \right| \le \varepsilon_1, \qquad \left| \frac{F_{k+1} - F_k}{F_{k+1}} \right| \le \varepsilon_1 \tag{17}$$

When the required condition was fulfilled, it was important to check and/or modify the flexural rigidity of the segments $(EI)_i$. The rigidity of each segment was obtained only after calculating the relative angular displacement φ_i, the normal force N_i in each segment, and the corresponding length of each segment ds_i. The formulae are as follows

$$N_i = \frac{F_k}{2} \cdot sin(\psi_i + \varphi_i) - H_{a,k} \cdot cos(\psi_i + \varphi_i) \tag{18}$$

$$d\varphi_i = \frac{\varphi_{i+1} - \varphi_{i-1}}{2 \cdot ds_i}, \tag{19}$$

$$ds_i = ds_{0,i} \cdot \left(1 + \frac{N_i}{EA_i}\right) \tag{20}$$

These values were required to calculate the effective flexural rigidity of each arch segment $(EI)_i$. Fig. 15 shows the curves of effective flexural rigidity EI for the P-28 profile for different values of the normal force. The values were obtained using FEM by Markopoulos *et al.* (2010).
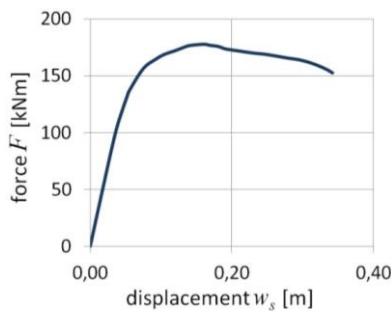
For the purposes of calculation, the values were arranged in a table. The effective flexural rigidity of the ith segment $(EI)_i$ was calculated directly as a function of N_i a dφ_i or by interpolation.

If it was necessary to change the rigidity in at least one segment, then the calculation was repeated until the rigidity was obtained for each segment. Next, the new values of the response H_a and force F were obtained and, if necessary, the rigidity of segments was modified.

The calculation was completed for the specified displacement w_s, if the displacement u_b was close to zero and the accuracy corresponded to ε_2, pursuant to the following

$$|u_{b,k}| \le \varepsilon_2, \qquad |w_{s,k} - w_s| \le \varepsilon_2, \tag{21}$$

Next, the process continued with increases in the displacement w_s. The entire process was repeated until the specified maximum displacement $w_{s,max}$ was reached.

5.1 Example

The load was applied in the above-described manner to a steel arch support used for mines. The arch support consisted of three overlapping circular arches composed of the P-28 profile. Table 2 shows the dimensions and overlapping length of the arches.

The support was divided into $n = 80$ segments. The geometry of the support was determined following the approach described by Janas *et al.* (2016). The analysis was performed using the minimum accuracy $\varepsilon_1 = 10^{-4}$ (the accuracy for determining the forces F, H_a, and H_b) and $\varepsilon_2 = 10^{-4}$ [m] (the accuracy for determining the displacement $u_{b,k}$ and $w_{s,k}$). As indicated by Fig. 18(a), the calculated F first increased with the increases in the deformation load until F_{max} was reached. Subsequently, F began decreasing, and this was primarily due to the decrease in the flexural rigidity at the top of the arch (as shown in Fig. 18(b)).

Table 2 Parameters of the mine support made from the P-28 profile

Length of the segment L_d [m]	3.65	2.65	3.65
Diameter of the segment R_d [m]	3.15	2.78	3.15
Overlapping of the segments p_d [m]	0.4	0.4	-

(a) The force-displacement diagram
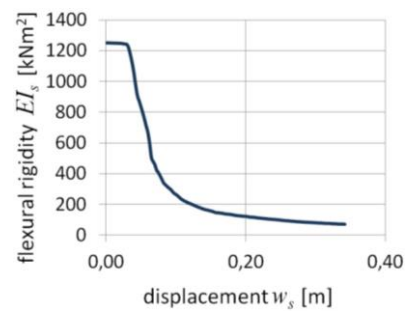
(b) Flexural rigidity vs. displacement w_s

Fig. 18 The force-displacement diagram and diagram of flexural rigidity vs. displacement w_s

6. Applying the virtual unit moments that load the arch support with passive forces

The loading of steel arch supports in long workings can be (in principle) active or passive. The active load was the result of the weight of loose ground, and it could result from the active deformation of a rock. It could also develop from the weight of the technology plant. The active loading caused the arch to deform. If the steel arch support was in contact with the rock, then the passive load was deformed due to the active loads of the arch. Typically, the passive forces very positively influence the load-carrying capacity
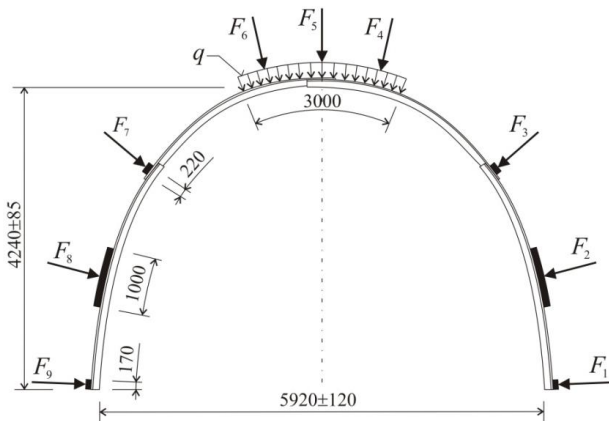
Fig. 19 The scheme of loading for steel arch support SP 16/4
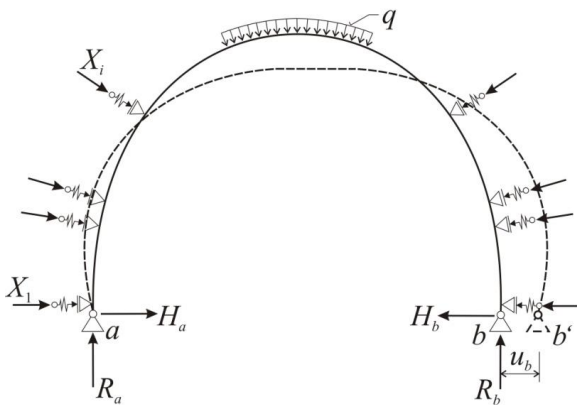
Fig. 20 The scheme of the steel arch support

of the arch support. This stabilizes the arch by inducing more positive components of the internal forces.

A test of the mining steel arch supports was conducted in GIG Katowice in 2012 (Paczesniowski 2012). The arch SP16/4 with an open TH-29 profile and H500M steel in the unyielding implementation was tested as shown in Fig. 19. The testing equipment enabled the simulation and measurement of a static loading of arch supports due to the pressure of the surrounding rocks. The unyielding steel arch support was exposed to both forces, namely active and passive forces. The active forces were made up of a uniform continuous load. The active forces were induced by the hydraulic presses that operated near the top of the arch perpendicular to the centerline at a length of 3 m. The passive forces acted from the right side respectively from the left side of the arch (Koubova *et al.* 2016).

The statically indeterminate horizontal response H_b was a function of the displacement u_b in the right support (see Eq. (16)). The uniform continuous load q was a function of the vertical displacement w_s. The secant method was also used to calculate the passive forces. The passive force X_i was a function of the displacement δ_i (it corresponded to the displacement in the direction of passive force)

$$X_{i,k+1} = X_{i,k} - \left[\delta_{i,k} - \left(-\frac{X_{i,k}}{c \cdot b \cdot ds_i}\right)\right] \cdot \frac{X_{i,k} - X_{i,k-1}}{\delta_{i,k} - \delta_{i,k-1}}. \quad (22)$$

In this equation, c denotes modulus of compressibility, b denotes width of the arch profile, and ds denotes the length of the adjacent arch segment.

It was necessary to check whether the resulting passive forces were not in tension. This was because the tension forces cannot generally occur in the support contact points. The tension passive forces are neglected in solution as follows. The results of numerical modeling indicated a very good agreement with the results obtained by the experimental load tests in the case of limited deformations (as shown in Fig. 21). The results of the numerical modeling could not be compared with the results of the experiment in the case of larger deformations. The value of the displacement almost reached 200 mm. It was limited by methodological procedures applied on the test set-up.

This study discussed examples of the nonlinear analyses of structures using a method of virtual unit moments and effective flexural rigidity. The method was first used with respect to a fixed rod with ideal elastic behavior. The results were compared with the accurate data. The findings
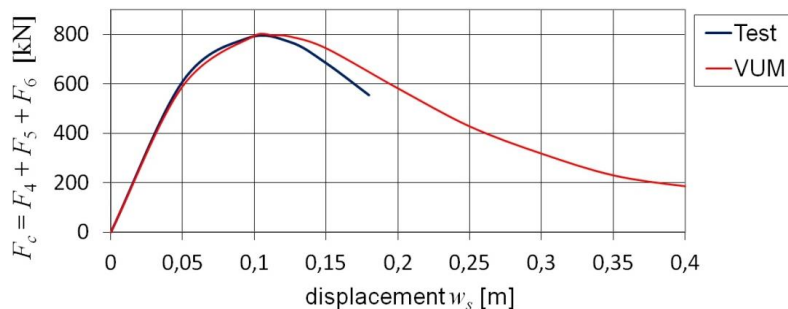
Fig. 21 Comparison of the test results and the results of numerical modeling

indicated that a high correlation existed.

The method was next applied to geometric and physical nonlinearities in open rolled profiles. The approach included the distribution of the modeling on two levels. The values of effective flexural rigidity were obtained by FEM modeling by ANSYS software at the first level. In the second level, the beams and arch supports were solved using effective flexural rigidity, virtual unit moments, and secant method. It should be noted that Visual Basic (which is a part of Microsoft Excel) was used for the analysis. The results of the bending test experiments were derived with respect to the known effective flexural rigidity of the open P-28 profile. The mining steel arch support loaded with a vertical force and the unyielding steel arch support exposed to active and passive forces were specifically focused on the study.

The use of the proposed method made it possible to obtain the solution for the "after-critical" condition when deformation increased with decreasing loads. The analysis was performed for statically determinate and indeterminate structures. The results proved that the virtual unit moments could be used for the geometric and physical nonlinear tasks in which displacement with respect to the size of the structure could not be ignored. These outcomes were possible if the effective flexural rigidity of the profile rod was known.

Acknowledgments

References

Bradford, M.A. (2006), "In-plane nonlinear behaviour of circular pinned arches with elastic restraints under thermal loading", *Int. J. Struct. Stabil. Dyn.*, **6**(2), 163-177.
https://doi.org/10.1142/S0219455406001897

Grochol, P. (1996), Assessment of the functional properties of the profiles K-21, K-24 and P-28, B 00575, Scientific Research Coal Institute, a.s. Ostrava-Radvanice, Czech Republic.

Heidarpour, A., Abdullah, A.A. and Bradford, M.A. (2010), "Non-linear inelastic analysis of steel arches at elevated temperatures", *J. Constr. Res.*, **66**, 512-519.
https://doi.org/10.1016/j.jcsr.2009.10.003

Janas, P. (2008), "The steel arc reinforcement in the long mining works, current options its assessment and dimensioning", *Proceedings of the traditional international geomechanical and geophysical scientific conference*, Ostravice, Czech Republic.

Janas, P., Kolos, I. and Fojtik, R. (2014), "Classification of steel mine support sections as per EC3 classification", *Adv. Mater. Res.*, **969**, 63-66.
https://doi.org/10.4028/www.scientific.net/AMR.969.63

Janas, P., Koubova, L. and Krejsa, M. (2016), "Load carrying capacity of steel arch reinforcement taking into account the geometrical and physical nonlinearity", *Appl. Mech. Mater.*, **821**, 709-716.
https://doi.org/10.4028/www.scientific.net/AMM.821.709

Janas, P., Janas, K., Koubova, L. and Krejsa, M. (2017),

"Modelling of Closed Steel Supports for Underground and Mining Works", *Key Eng. Mater.*, **754**, 313-316.
https://doi.org/10.4028/www.scientific.net/KEM.754.313

Kala, Z., Kalina, M. and Frantik, P. (2015), "Buckling and post-buckling of the von mises planar truss", *AIP Conference Proceedings*, **1648**, 1-4.

Kolar, V. (1985), *Nonlinear Mechanics*, House Technology CSVTS, Ostrava, Czech Republic.

Koubova, L., Janas, P. and Krejsa, M. (2016), "Nonlinear solution of steel arch supports", *Key Eng. Mater.*, **713**, 119-122.
https://doi.org/10.4028/www.scientific.net/KEM.713.119

Kralik, J. (2014), "A RSM approximation in probabilistic nonlinear analysis of fire resistance of technology support structures", *Adv. Mater. Res.*, **969**, 1-8.
https://doi.org/10.4028/www.scientific.net/AMR.969.1

Krejsa, M., Janas, P., Yilmaz, I., Marschalko, M. and Boucha, T. (2013), "The use of the direct optimized probabilistic calculation method in design of bolt reinforcement for underground and mining workings", *Sci. World J.*, **2013**.
http://dx.doi.org/10.1155/2013/267593

Ma, J., Liu, Y., Gao, Q. and Hou, K. (2015), "Investigating the hysteretic behaviour of concrete-filled steel tube arch by using a fiber beam element", *Math. Probl. Eng.*, **15**, 1-7.
http://dx.doi.org/10.1155/2015/409530

Markopoulos, A., Janas, P. and Podesva, J. (2010), "Alternative flexural rigidity of the profile P-28 with axial force", *Proceedings of International Conference Modelling in Mechanics*, **2010**, 1-7.

Mattiasson, K. (1981), "Numerical results from large deflection beam as frame problems analyzed by means of elliptic integral", *Int. J. Numer. Method. Eng.*, **17**(1), 145-153.

Paczesniowski, K. (2012), Test of mining steel arch support type SP 16/4, BL-2/12-50, Group of the testing and calibration laboratories of the mining general institut (GIG), Katowice, Poland.

Pi, Y.L. and Bradford, M. (2010), "Effects of prebuckling analyses on determining buckling loads of pin-ended circular arches", *Mech. Res. Commun.*, **37**, 545-553.
https://doi.org/10.1016/j.mechrescom.2010.07.016

Pi, Y.L. and Bradford, M. (2013), "Nonlinear analysis and buckling of shallow arches with unequal rotational end restraints", *Eng. Struct.*, **46**, 615-630.
https://doi.org/10.1016/j.engstruct.2012.08.008

Pi, Y.L. and Trahair, N. (2000), "Inelastic lateral buckling strength and design of steel arches", *Eng. Struct.*, **22**, 993-1005.
https://doi.org/10.1016/S0141-0296(99)00032-2

Pi, Y.L., Bradford, M. and Uy, B. (2002), "In-plane stability of arches", *Int. J. Solids Struct.*, **39**, 105-125.
https://doi.org/10.1016/S0020-7683(01)00209-8

Randyskova, L. and Janas, P. (2010), "Bending test-based determination of effective cross-section stiffness", *Transactions of the VSB-Technical University of Ostrava, Civil Engineering Series*, **10**(1), 1-8.

Randyskova, L. and Janas, P. (2011), "Nonlinear solution of steel arch reinforcement with influence of passive forces", *Transactions of the VSB-Technical University of Ostrava, Civil Engineering Series*, **11**(1), 1-6.

Starossek, U., Falah, N. and Lhning, T. (2010), "Numerical analyses of the force transfer in concrete-filled steel tube", *Struct. Eng. Mech., Int. J.,* **35**(2), 241-256.
https://doi.org/10.12989/sem.2010.35.2.241

Xu, T., Xiang, T., Zhao, R. and Zhan, Y. (2010), "Nonlinear finite element analysis of circular concrete-filled steel tube structures", *Struct. Eng. Mech., Int. J.*, **35**(3), 315-333.
https://doi.org/10.12989/sem.2010.35.3.315

BU